Synthesis of Nanoporous Type A and X Zeolite Mixtures from Biomass Combustion Fly Ash for Post-Combustion Carbon Capture

Ben Petrovic[1], Mikhail Gorbounov[1], Serap Özmen[2], Peter Clough[2] and Salman Masoudi Soltani[1]

[1]Department of Chemical Engineering, Brunel University London, Uxbridge UB8 3PH, United Kingdom

[2]Energy and Power Theme, School of Water, Energy and Environment, Cranfield University, Cranfield MK43 0AL, United Kingdom

Abstract — **In this study, improved nanoporous zeolites for use in post-combustion carbon capture have been synthesised from industrial-grade biomass combustion fly ash generated in one of the largest biomass combustion power plants in the UK. The method of nanoporous zeolite synthesis follows an alkaline fusion-assisted hydrothermal procedure. The nanoporous zeolites have been characterised by scanning electron microscopy (SEM), energy dispersive X-ray spectroscopy (EDS), X-ray diffraction (XRD) and Fourier-transform infrared spectroscopy (FTIR). The presence of two crystalline structures, Faujasite and Linde Type A has been confirmed by the characterisation results. The CO_2 adsorption investigations were conducted *via* thermogravimetric analysis (TGA) to estimate the uptake capacity of the prepared adsorbents. TGA studies suggest that the improved nanoporous adsorbent, evaluated under 100 mol% CO_2 at atmospheric pressure, has an equilibrium capacity of over 1.6 $mmol_{CO2}/g$ at 50 °C, a two-fold increase from our previous study with a crystalline structure confirmed by XRD.**

I. INTRODUCTION

With the 26th UN Climate Change Conference of the Parties recently behind us, the global drive to net-zero greenhouse gas emissions is distinctly apparent and of the utmost importance. With around 85 % of the global energy demand sourced from the combustion of fossil fuels [1], there are three conventionally adopted routes to developing sustainable energy policy, hence distancing this industry from the use of fossil fuels. These are the improvement of process efficiency, finding alternative fuel sources and carbon capture and storage (CCS). The first two routes are well documented but have plateaued without any significant recent developments. The third has the largest scope for both deployment and practical utility; the Intergovernmental Panel on Climate Change have consistently identified CCS as essential in limiting global temperature increase. The UK's government have referred to CCS as a breakthrough technology featuring exclusively as the 8th point in the 10-point plan announced in November 2020 to accelerate a green revolution [2], [3]. Adsorption-based processes are poised for significant development and thus, deployment in the field of post-combustion carbon capture (PCCC) due to their associated low energy requirement, high efficiency and environmental friendliness when compared to the conventional amine-based absorption processes [4], [5].

The viability of adsorption-based processes depends on the development of an adsorbent with good mechanical, chemical and cyclic stability, high uptake, fast kinetics and a relatively low cost. Within the arsenal of solid porous materials that have potential for deployment in these processes, the scale in which they are required often makes their cost the limiting factor. Materials such as zeolite 5A [6], zeolite 13X [7] and activated carbon (AC) [8] have been widely investigated for CO_2 capture. Waste-derived sorbents such as coal fly ash-zeolites (FAZ) [9] have also been shown to be extremely promising for CCS processes by simultaneously adding value to a waste stream and removing the need for disposal. If these sorbents can be employed on the same site in which they are produced, the potential for cost-reduction is vast so long as the adsorbent properties and performance are sufficient.

II. MATERIALS AND METHODOLOGY

In this work, we have adopted an alkaline-fusion assisted hydrothermal procedure to synthesise a nanoporous zeolite mixture, using industrial biomass combustion fly ash (BFA) generated in the UK's largest thermal power plants as the precursor. NaOH (Sigma Aldrich, ≥97%) was used as the alkaline. With a view to improve both crystallinity and yield of the produced zeolite, the method from the previous work [10] was modified by increasing the ratio of NaOH to BFA. The method follows mixing the BFA (10 g) with NaOH (20 g, w/w = 2), and then grinding this for 5 mins in a pestle and mortar. This mixture was then fused in a muffle furnace by heating to 550 °C at 5 °C min^{-1} and holding for 1 hour. With the fusion product cooled to room temperature, 100 mL deionised water was then added to a TFM liner (Berghof DAB-3) to which the pulverised fusion product (15 g) was added. The solution was then magnetically stirred at 300 rpm and room temperature for 16 hrs on a magnetic hot plate stirrer (Fisherbrand Isotemp). Subsequently, the TFM liner was inserted into a stainless-steel pressure digestion vessel (Berghof DAB-3) and then treated hydrothermally by heating to 90 °C at 0.5 °C min^{-1} and holding for 4 hrs. Once the pressure vessel had cooled to room temperature, the TFM liner was removed and the solution decanted; the product was then washed with deionised water *via* vacuum filtration (No.1 9 cm) until a pH of 7 was reached in the filtrate. The zeolite

product was then dried overnight at 110 °C in an oven (Fisher Scientific Isotemp 825F).

The zeolite product has been characterised extensively by Scanning Electron Microscopy (SEM, LEO 1455VP), Energy Dispersive X-Ray Spectroscopy (EDS, Oxford INCAx-act), Fourier Transform Infrared spectrometry (FTIR, Perkin Elmer Spectrum One) and X-Ray Diffraction (XRD, Bruker D8). Surface area measurements have been carried out *via* the BET technique (3P Instruments) using nitrogen adsorption/desorption isotherms measured at 77 K; the sample was degassed at 350 °C for 2 hrs (ramp rate 10 °C min^{-1}). The CO_2 adsorption performance has been evaluated *via* thermal gravimetric analysis (TGA, Mettler Toledo TGA 2). The performance of the product was measured under isothermal conditions with a pure CO_2 (99.9 %) gas flow of 50 ml min^{-1} at atmospheric pressure. The initial purge was carried out at 150 °C under an N_2 atmosphere for 1 hr and the adsorption regime held for 2 hrs.

III. RESULTS AND DISCUSSION

A. Biomass Fly Ash-Derived Zeolite Characterisation

The zeolite morphology and crystal structure have been evaluated through SEM by first suspending the sample in isopropyl alcohol to disperse large aggregates into smaller fragments that have better contact with the conductive surface. The solution was then pipetted onto a copper plate; the dried sample was then gold coated to dissipate charging effects. The microscope images can be seen in Fig. 1. With an accelerating voltage of 15 kV, the crystal structure of the nanoporous zeolites can be clearly seen. Linde Type A (LTA) zeolites and Faujasite (FAU) zeolites both possess similar secondary building units: sodalite cages linked by double-four rings for LTA and double-six rings for FAU. Even with this, the unit cell of each crystal structure is quite dissimilar, under the SEM LTA structures present a cubic arrangement, whereas FAU a hexaoctahedral arrangement [11]. With this in mind, the images in Fig. 1 exhibit both cubic and octahedral morphology, along with a considerable amount of amorphous and non-crystalline aluminosilicate species; examples of these are indicated on Fig. 1 by blue (LTA) and green (FAU) rings

The XRD diffractogram (Fig. 2) was able to corroborate the findings from the SEM. Measured in a 2θ range of 5 – 90 °, the crystalline structures of the BFA-zeolite are apparent. LTA and FAU, given their similar building units, present diffraction patterns with some overlap. Even with this, there are characteristic peaks for each crystal structure. Present in the pattern is a broad background line elevation in the 2θ range of 15 – 35 °, characteristic of fly ash derived zeolites which is indicative of the presence of amorphous aluminosilicate species [12], [13], suggesting that the employed method has been unsuccessful in converting the amorphous precursor entirely into zeolite structures. Given the potential for synthetic zeolites to exchange cations, and the presence of a significant quantity of alkali and alkaline earth metals in the precursor, identification of the specific LTA (3A, 4A or 5A) or FAU (NaX, KX) phase is required.
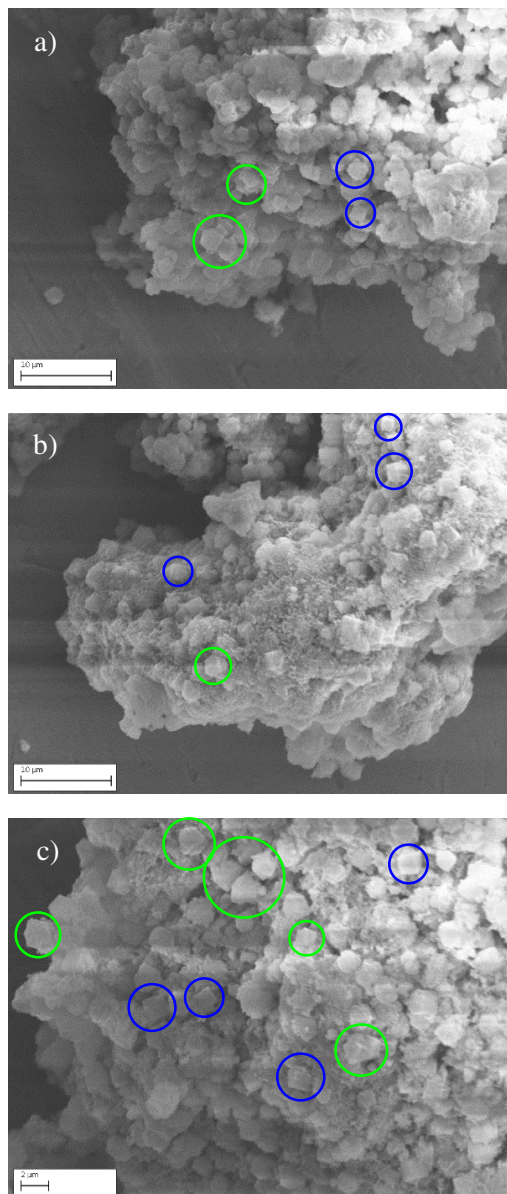

Fig. 1: SEM images of the BFA-derived zeolite obtained at 15kV and 50 pA: a) 5kx mag.; b) 5kx mag.; and c) 7.5kx
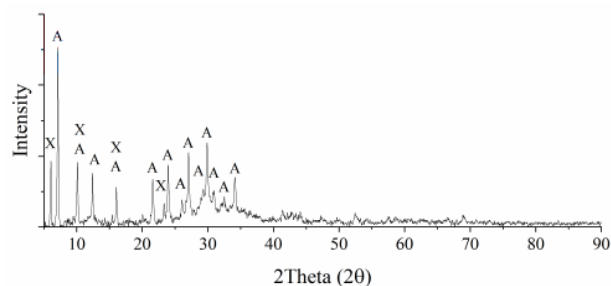

Fig. 2: X-ray diffractogram of the biomass-combustion fly ash-derived nanoporous zeolite.

Some evidence of the cation can be found in the diffractogram if the relevant peak intensity ratios and shifts are considered due to the difference in scattering power specific to each cation and the variation in site occupation [14], [15].

Table I: The elemental analysis (EDS)of the BFA-zeolites.

Element	Weight (%)
Na	4.15
Mg	1.70
Al	12.95
Si	20.90
K	0.95
Ca	12.05
Fe	3.45
O	43.90

Table II: Zeolite infrared assignments (cm^{-1}) reproduced from [17].

Internal Tetrahedra		External Tetrahedra	
Asymmetric Stretching	1250 – 950	Double Ring	650 – 500
Symmetric Stretching	720 – 650	Pore Opening	420 – 300
T-O Bend	500 - 420	Symmetric Stretching	820 – 750
		Asymmetric Stretching	1150 – 1050

By determining the average composition of the zeolite samples through consideration of several areas with EDS, the results (Table I) suggest that the zeolite phases present have an average silica to alumina ratio of 3.1. From the elevated concentration of calcium present in the sample, it can be inferred that the LTA structures present may be of the 5A type (calcium exchanged LTA) as the calcium ions, like those of sodium, take place as charge compensators in the frameworks [11]. Even with this, the presence of both sodium and potassium suggests that both 4A (sodium exchanged LTA) and 3A (potassium exchanged LTA) are also present. The sodium however, may be a residuum of the NaOH being used as the alkaline in this zeolite synthesis. Given that there still exist some amorphous species in the sample as evidenced in the SEM, the sodium observed may be present in the amorphous aluminosilicate species derived during the dissolution of the sodium-aluminosilicates formed during fusion rather than the crystalline structures.

The FTIR spectrum of the BFA-zeolite shown in Fig. 3was collected in the region of 4000 – 450 cm^{-1} after mixing the sample with KBr powder and pressing into a disk at 100 kN. As a result of the sample preparation, the peak centred at around 3500 cm^{-1} has been ascribed to the stretching vibration of -OH groups present in water on the materials surface [16]. Similarly, the two peaks at around 2900 cm^{-1} have been attributed to the sample preparation introducing impurities since these wave numbers are characteristic of aliphatic carbon and were observed in a pure KBr spectrum. The bands observed for zeolites in the mid infrared region are classified into two main categories, the first due to internal vibrations of the tetrahedra and the second, due to external vibrations of the tetrahedra linkages [17], [18] such as the double rings in LTA
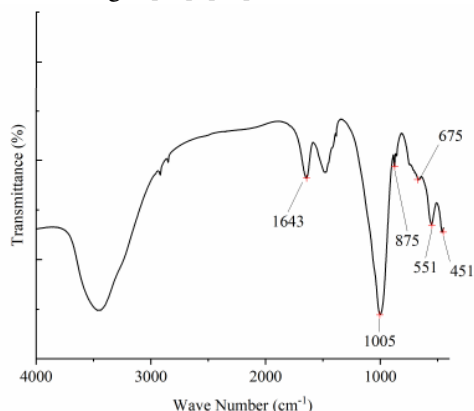
and FAU. The internal vibrations are known to be insensitive to structure; the external vibrations however, are indicative of the structure type. Table II exhibits the typical assignments.

The spectrum in Fig. 3 is characterised by the bands typical for both LTA and FAU type zeolite structures [12], [19]. The band centred at 1643 cm^{-1} is characteristic of -OH group bending vibrations often defined as the 'zeolitic' water [12] found in hydrated zeolites. The wave number region of 1090 – 900 cm^{-1} is related to the internal asymmetric stretching vibrations of the Si-O-T bridges [12], [16] where T can be either Si or Al. The shift of this frequency to 1005 cm^{-1} from around 1100 cm^{-1} for pure silica is due to a decrease in the framework Si/Al [20] as the length of the Al-O bond is 1.73 Å, whereas the Si-O bond is 1.62 Å. The band seen at 675 cm^{-1} is related to the symmetric stretching of Si-O-Al bridges, whilst the band at 551 cm^{-1} is characteristic of the symmetric Si-O-Si stretching and O-Si-O bending vibrations of the double rings [12], [21].

B. CO$_2$ Adsorption Performance

Improving from the previous research study, the nanoporous zeolite as confirmed by XRD, SEM and FTIR has a significantly improved equilibrium uptake of CO$_2$ at 50 °C. Notably, there is a significant initial uptake to around 1 mmol$_{CO2}$/g within the first ten minutes. Thereafter, the equilibrium capacity of the zeolite reaches 1.66 mmol$_{CO2}$/g after two hours; a two-fold increase to that reported in the previous study (0.825 mmol$_{CO2}$/g) [10]. By considering the BET surface area of 73.95 m^2 g^{-1}, the ability for it to adsorb this amount is encouraging and suggests that BET surface area measurements fail to directly correlate to adsorption capacity. Fig. 4 indicates three distinct regions on the adsorption curve. This can imply different diffusional mechanisms taking place. The first region (<5 mins)
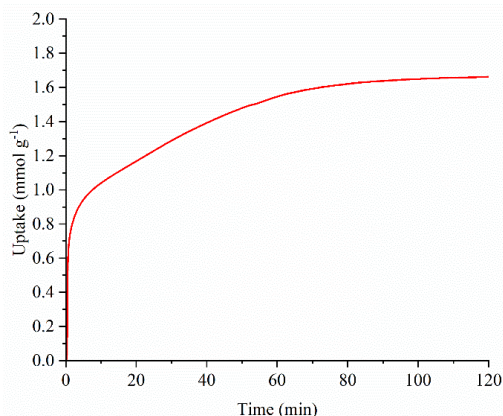

Fig. 3: Fourier-Transform Infrared Spectrum of the prepared biomass combustion fly ash-derived zeolite.

Fig. 4: CO$_2$ adsorption curve of the biomass-combustion fly ash-derived zeolite.

representing the initial bulk diffusion; this is followed by the intraparticle diffusion of CO_2 between 5 to 60 mins; the third region is the equilibration of the adsorption process as CO_2 finds a final adsorption site within the nanoporous network defined as surface diffusion [22], [23]. At present, limited modelling of the adsorption kinetics has been made to reveal the various mechanisms at play; this information, along with the equilibrium isotherms for CO_2 and N_2 will inform the feasibility of biomass combustion ash-derived nanoporous zeolites for deployment in PCCC

IV. CONCLUSION

A crystalline nanoporous zeolitic adsorbent for CO_2 capture has been produced from biomass combustion fly ash through an alkaline fusion-assisted hydrothermal procedure. The characterisation results clearly demonstrate a partial conversion of the amorphous fusion intermediate to crystalline phases of Linde Type A and Faujasite zeolites. The equilibrium CO_2 uptake of 1.66 mmol g^{-1} at 50 °C is double that of our previous work and clearly demonstrates that crystalline zeolitic phases with potential for post-combustion carbon capture can be produced from this waste stream. With subsequent assessment of the CO_2 adsorption mechanisms and tailoring of the synthesis method, the viability of this route for biomass ash valorisation can be revealed.

REFERENCES

[1] M. Younas et al., "Recent progress and remaining challenges in post-combustion CO2 capture using metal-organic frameworks (MOFs)," *Prog. Energy Combust. Sci.*, vol. 80, p. 100849, 2020.

[2] S. Masoudi Soltani, A. Lahiri, H. Bahzad, P. Clough, M. Gorbounov, and Y. Yan, "Sorption-enhanced Steam Methane Reforming for Combined CO2 Capture and Hydrogen Production: A State-of-the-Art Review," *Carbon Capture Sci. Technol.*, vol. 1, no. August, p. 100003, 2021.

[3] United Kingdom HM Government, "The Ten Point Plan for a Green Industrial Revolution," *Dep. Business, Energy Ind. Strateg.*, no. November, 2020.

[4] B. Petrovic, M. Gorbounov, and S. Masoudi Soltani, "Influence of surface modification on selective CO2 adsorption: A technical review on mechanisms and methods," *Microporous Mesoporous Mater.*, no. October, p. 110751, Nov. 2020.

[5] R. M. Firdaus, A. Desforges, A. Rahman Mohamed, and B. Vigolo, "Progress in adsorption capacity of nanomaterials for carbon dioxide capture: A comparative study," *Journal of Cleaner Production*, vol. 328. 2021.

[6] P. A. P. Mendes, A. M. Ribeiro, K. Gleichmann, A. F. P. Ferreira, and A. E. Rodrigues, "Separation of CO2/N2 on binderless 5A zeolite," *J. CO2 Util.*, vol. 20, 2017.

[7] Y. Park, Y. Ju, D. Park, and C. H. Lee, "Adsorption equilibria and kinetics of six pure gases on pelletized zeolite 13X up to 1.0 MPa: CO2, CO, N2, CH4, Ar and H2," *Chem. Eng. J.*, vol. 292, 2016.

[8] P. Ammendola, F. Raganati, and R. Chirone, "CO2 adsorption on a fine activated carbon in a sound assisted fluidized bed: Thermodynamics and kinetics," *Chem. Eng. J.*, vol. 322, 2017.

[9] S. Boycheva et al., "Progress in the Utilization of Coal Fly Ash by Conversion to Zeolites with Green Energy Applications," *Materials (Basel).*, vol. 13, no. 9, p. 2014, 2020.

[10] B. Petrovic, M. Gorbounov, A. Lahiri, and S. Masoudi Soltani, "Biomass Combustion Fly Ash-Derived Nanoporous Zeolites for Post-Combustion Carbon Capture; Biomass Combustion Fly Ash-Derived Nanoporous Zeolites for Post-Combustion Carbon Capture," 2021.

[11] S. Boycheva, D. Zgureva, H. Lazarova, and M. Popova, "Comparative Studies of Carbon Capture onto Coal Fly Ash Zeolites Na-X and Na-Ca-X," *Chemosphere*, vol. 271, p. 129505, 2021.

[12] R. Panek, J. Madej, L. Bandura, and G. Słowik, "Recycling of waste solution after hydrothermal conversion of fly ash on a semi-technical scale for Zeolite synthesis," *Materials (Basel).*, vol. 14, no. 6, pp. 1–16, 2021.

[13] O. Babajide, N. Musyoka, L. Petrik, and F. Ameer, "Novel zeolite Na-X synthesized from fly ash as a heterogeneous catalyst in biodiesel production," *Catal. Today*, vol. 190, no. 1, 2012.

[14] L. Price, K. M. Leung, and A. Sartbaeva, "Local and average structural changes in zeolite a upon ion exchange," *Magnetochemistry*, vol. 3, no. 4, 2017.

[15] A. J. Chandwadkar, J. G. Chandwadkar, and S. B. Kulkarni, "The influence of the size and concentration of alkaline earth ions on the structural and sorption properties of faujasites," *J. Colloid Interface Sci.*, vol. 97, no. 2, 1984.

[16] Y. Wang, T. Du, X. Fang, H. Jia, Z. Qiu, and Y. Song, "Synthesis of CO2-adsorbing ZSM-5 zeolite from rice husk ash via the colloidal pretreatment method," *Mater. Chem. Phys.*, vol. 232, no. April, pp. 284–293, 2019.

[17] E. M. FLANIGEN, H. KHATAMI, and H. A. SZYMANSKI, "Infrared Structural Studies of Zeolite Frameworks," 1974.

[18] H. G. Karge, M. Hunger, and H. K. Beyer, "Characterization of Zeolites — Infrared and Nuclear Magnetic Resonance Spectroscopy and X-Ray Diffraction," in *Catalysis and Zeolites*, 1999.

[19] M. Król, W. Mozgawa, W. Jastrzbski, and K. Barczyk, "Application of IR spectra in the studies of zeolites from D4R and D6R structural groups," *Microporous Mesoporous Mater.*, vol. 156, 2012.

[20] M. Gorbounov, B. Petrovic, A. Lahiri, and S. Masoudi Soltani, "Application of Nanoporous Carbon, Extracted from Biomass Combustion Ash, in CO2 Adsorption;

[21] H. Tounsi, S. Mseddi, and S. Djemel, "Preparation and characterization of Na-LTA zeolite from Tunisian sand and aluminum scrap," *Phys. Procedia*, vol. 2, no. 3, 2009.

[22] N. Álvarez-Gutiérrez, M. V. Gil, F. Rubiera, and C. Pevida, "Kinetics of CO2 adsorption on cherry stone-based carbons in CO2/CH4 separations," *Chem. Eng. J.*, vol. 307, pp. 249–257, 2017.

[23] S. Loganathan, M. Tikmani, S. Edubilli, A. Mishra, and A. K. Ghoshal, "CO2 adsorption kinetics on mesoporous silica under wide range of pressure and temperature," *Chem. Eng. J.*, vol. 256, 2014.

Synthesis of nanoporous type A and X zeolite mixtures from biomass combustion fly ash for post-combustion carbon capture

Petrovic, Ben

Petrovic B, Gorbounov M, Özmen S, Clough P & Soltani SM (2022) Synthesis of nanoporous type A and X zeolite mixtures from biomass combustion fly ash for post-combustion carbon capture. In: 2022 IEEE 22nd International Conference on Nanotechnology (NANO), 4-8 July 2022, Palma de Mallorca